Ground-state Lennard-Jones and Aziz boson liquids: Perturbation theory and computer experiment

Christina Keller, M. de Llano, and S. Z. Ren*
Physics Department, North Dakota State University, Fargo, North Dakota 58105

E. Buendía and R. Guardiola
Departmento de Física Moderna, Universidad de Granada, E-18071 Granada, Spain
(Received 30 May 1989)

The exact, low-density many-boson expansion for the ground-state energy is rearranged in a quantum-thermodynamic perturbation series. Extrapolation to physical densities is implemented order by order via Padé-type approximants. Several ways of splitting the pair Lennard-Jones (LJ) or Aziz potentials are considered, including the Barker-Henderson (BH) and Weeks-Chandler-Andersen (WCA) schemes familiar from classical fluid studies. Results obtained using the LJ interaction with WCA splitting, when compared with benchmark simulation data, agree excellently in energy and density, but only moderately so in sound velocity. For the Aziz potential, however—perhaps because of a softer core and/or its ability to support a two-particle bound state—, neither potential splitting (BH or WCA) gave results of the LJ quality, but a method intermediate between BH and WCA proves to be superior. Our results are also compared with other recent alternative calculations, both variational and perturbative.

I. INTRODUCTION

An important first step in understanding any liquid is to be able to calculate from first principles its ground-state energy and equilibrium density. To obtain the ground-state energy per particle, one need only solve the corresponding Schrödinger equation, which, unfortunately, is exactly soluble only for very few model Hamiltonian many-body systems. For a more or less realistic model, one must resort to some approximation scheme capable of providing an accurate value for the energy and density.

Several approaches have been applied to the problem of liquid ^{4}He. Most of these may be grouped into two general categories, *variational*[1] or *perturbative* in nature. A scheme which falls into neither the variational nor the perturbative category is the Green-function Monte Carlo (GFMC) method.[2] This method gives "exact" computer experimental results for a fixed number of particles since the experimenter has full control of the interparticle interaction—an advantage rarely had in actual laboratory experiments. Thus, theoretical calculations are ideally compared to GFMC results, when available.

In most cases the Hamiltonian takes the form

$$\hat{H} = -\sum_{i=1}^{N} \frac{\hbar^2}{2m}\nabla_i^2 + \sum_{i<j}^{N} V(\mathbf{r}_{ij}) , \tag{1}$$

where $V(\mathbf{r}_{ij})$ is some appropriate interparticle potential. In the perturbative approach, the interaction term in the Hamiltonian (1) is multiplied by a strength parameter λ, $0 \le \lambda \le 1$, with $\lambda = 1$ giving the full Hamiltonian. One of the several perturbation methods is based on the so-called "parquet" diagrams,[3] a self-consistent sum of particle-particle and particle-hole diagrams. As such, the well-known "ring" as well as "ladder" diagrams are included. These "full" parquet diagrams provide a formidable numerical challenge so various simplifying assumptions are made. The dressed propagators are replaced by free propagators, the two-particle vertices are considered a function of three-momentum transfer rather than nine, and a further approximation for the free propagator is made. Since gross underbinding results, corrections must be made to the propagators to achieve an acceptable energy per particle. Using these corrections, a reasonable value for the energy emerges.

Another method is the exponential-S or coupled-cluster method (CCM) originally developed by Coester and Kümmel *et al.*,[4] and recently reviewed by Bishop and Kümmel.[5] Initially designed for nuclear physics, and later reapplied to problems in condensed-matter physics and quantum chemistry, this scheme attempts to avoid diagrams and approximations as far as possible. Initial applications of this method to liquid ^{3}He and ^{4}He were disappointing, resulting also in gross underbinding.[6] This was explained by the fact that, while in a low-density system two- or at most three-body excitations may be all that predominate, in a liquid the interparticle spacing is small so that the chance that groups of more than three particles are excited increases. Extensions of this elegant method are presently being pursued in an attempt to remedy this underbinding.

Employing the techniques of quantum field theory through an infinite partial summation of Feynman diagrams, one may obtain[7] for the ground-state energy an asymptotically exact nonpower series in the density. Only the first few terms of this series have been calculated due to the increasing complexity of the integrals involved in evaluating the successive "virial-like" coefficients. While this is satisfactory for a low-density system where the terms are rapidly convergent, such is

not the case for the liquid phase at higher densities. Fortunately, there exist extrapolation techniques which allow one to handle such slowly convergent (and even divergent) series. We will examine how one may apply such techniques, particularly the method of Padé approximants, to obtain excellent results for the energy per particle, equilibrium density, and sound speed in the liquid ^{4}He ground state. The perturbative method now to be described has, we believe, two advantages over previous methods: (1) it exploits the maximum available rigorous many-body information for a given pair potential, and (2) in predicting the properties of the liquid state, it explicitly avoids[8] crossing phase boundaries, specifically the one separating the single-phase gas from the two-phase gas-liquid regions.

II. REARRANGEMENT OF THE LOW-DENSITY SERIES

In applying the techniques of quantum field theory to the many-boson system of ^{4}He atoms several problems unique to the Bose system are encountered. Since bosons do not obey an exclusion principle, all the particles in a noninteracting system are in a single-particle state, namely the one with zero linear momentum. Switching on an interparticle interaction will excite some particles out of this zero-momentum condensate, thus reducing the occupancy of the lowest state. This depletion effect is negligible for a very low-density system. The average interparticle spacing is large and the probability that two particles will interact via a short-ranged potential and be excited out of the condensate remains small. At intermediate (i.e., physical) densities this is of course not so. A second difficulty peculiar to the *boson* case is that third- and higher-order perturbative corrections to the unperturbed energy diverge[7] even for a well-behaved, nonsingular potential. This divergence can be handled by applying infinite partial summation (renormalization) techniques to the series, which leave a finite but nonanalytic expansion in the density.

For example, to find the leading correction in the expression for the energy per particle, one need only evaluate $\frac{1}{2}\rho v(0)$, where $v(0)\equiv\int d^3r\, V(r)$ is just the volume integral of the pair potential, $V(r)$. But, if $V(r)$ is singular then $v(0)$ is infinite and the result is clearly useless. Using diagrammatic perturbation theory to sum terms to infinite order, however, one can choose certain selected classes of diagrams to be retained. The most divergent set of diagrams (i.e., the so-called "ladder" diagrams) are summed with the use of a Bethe-Salpeter-like integral equation. The divergent leading term $\frac{1}{2}\rho v(0)$ is now replaced by the so-called Lenz term, $2\pi\hbar^2\rho a/m$, where a is the (in general finite) S-wave scattering length associated with the pair potential (which may or may not be finite). Continuing with these techniques and summing to infinite order in each step the set of next most divergent diagrams, the resultant finite but nonanalytic expansion for the energy per particle is[7]

$$\frac{E}{N}=\frac{2\pi\hbar^2\rho a}{m}[1+C_1(\rho a^3)^{1/2}+C_2(\rho a^3)\ln(\rho a^3) +C_3(\rho a^3)+O((\rho a^3)^{3/2}\ln(\rho a^3))]\ . \tag{2}$$

This is evidently *not* a power series in ρ, nor even in the obvious smallness expansion parameter $(\rho a^3)^{1/2}$. The coefficients C_1 and C_2 are the pure numbers

$$C_1=128/(15\sqrt{\pi})\cong 4.814\,418\ ,\qquad C_2=8(4\pi/3-\sqrt{3})\cong 19.653\,92\ , \tag{3}$$

whereas C_3 is associated with real three-body cluster diagrams and therefore potential-shape dependent. The coefficient C_3 has never been calculated. Evaluating higher-order corrections to the expansion is difficult due to the increasing number and complexity of the integrals. In fact, the effort required to evaluate each subsequent term in the series is usually greater than the total effort of calculating all previous contributions. The series (2) can then be considered as a sequence of smaller and smaller corrections to the ideal Bose gas at zero absolute temperature. The first of these corrections, the Lenz term, represents the energy increase due to an "excluded volume" effect. Subsequent terms are harder to interpret physically, but are otherwise exact corrections.

Table I gives the S-wave scattering lengths[9] a for the Lennard-Jones (LJ) and Aziz He-He potential, as well as the corresponding scattering lengths a_0 of the associated Weeks-Chandler-Andersen (WCA) reference potential (see below), both in Å units. The large, negative a value for the LJ potential results from an attractive well which nearly binds an S state. Negative a values in (2), of course, are meaningless. For the Aziz potential a is large and positive (revealing a shallow two-body bound state). A graph of the energy per particle as given by (2) with this value of a is shown in Fig. 1 (thin curve): the energy is positive and *9 orders of magnitude* too high with respect to either the empirical equilibrium energy-density value (dot) or the GFMC results (squares). The low-density expansion[2] is clearly useless as it stands.

TABLE I. Comparison of the scattering lengths a and critical value λ of the strength parameter for the LJ and Aziz potentials required to bind zero-energy S-wave level. Both of these potentials are split using the WCA scheme, with a_0 corresponding to the repulsive part.

	LJ	Aziz
a	−176.325290 Å	+125.081 004 Å
λ_c	≃1.014296	≃0.982227
a_0	2.138 238 Å (WCA)	2.203 290 Å (WCA)
a/a_0	−82.459 421 57 (WCA)	56.770 104 71 (WCA)

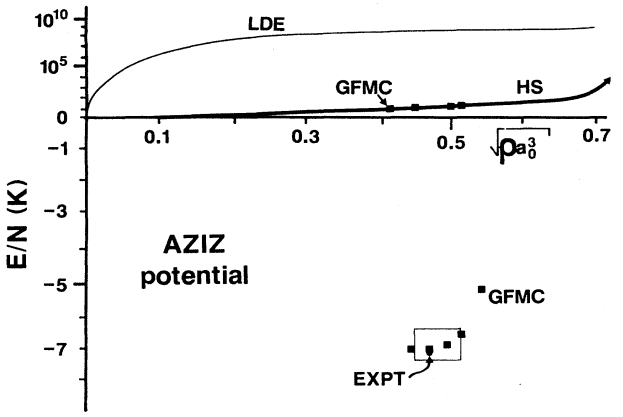

FIG. 1. Energy per particle as a function of $(\rho a_0^3)^{1/2}$, with ρ the particle density and a_0 defined in Eq. (5) for the BH splitting of the Aziz pair potential as discussed in text. The thin curve labeled LDE refers to the low-density expansion exactly as given in Eq. (2), but without the unknown C_3 term. The thick curve is the hard-sphere (HS) equation of state ϵ_0/N part of (6), with $e_0(x)$ replaced by (23). Squares denote the GFMC data and the dot refers to the experimental value for the zero-pressure equilibrium point. The box near the experimental value refers to the range of densities and energies encompassed in Figs. 11 and 12, which together summarize our final calculational results. Note that positive and negative energy scales differ drastically.

From both classical and quantum computer simulations,[2] the pair distribution function for the Lennard-Jones interaction, for example, is qualitatively similar to that of a fluid of purely repulsive cores. This suggests that the expansion (2) be rearranged by defining a coupling parameter $0 \le \lambda \le 1$ such that

$$V(r) = V_{\text{ref}}(r) + \lambda V_{\text{att}}(r) , \tag{4}$$

where the "reference" potential $V_{\text{ref}}(r)$ contains most of the repulsion, and $V_{\text{att}}(r)$ most of the attraction. Thus, instead of splitting the Hamiltonian into kinetic and potential energy terms, as implied by the original perturbation scheme leading to (2), some of the interaction is included in the reference system. Various partitioning methods can be tried and will be detailed later. The total scattering length can now be written formally as a power series in the new expansion parameter λ, namely

$$a = a_0 + a_1\lambda + a_2\lambda^2 + \cdots \equiv a_0 \left[1 + \sum_{i=1}^{\infty} \alpha_i \lambda^i \right] , \tag{5}$$

with a_0 the scattering length of $V_{\text{ref}}(r)$ alone. Substituting this expansion for a into (2) and rearranging leads to a new expression for the energy per particle, which is a double series in density and in attractive strength given by

$$\begin{aligned} E/N &= \frac{2\pi\hbar^2}{m a_0^2} x^2 \sum_{j=0}^{\infty} \alpha_j e_j(x) \lambda^j \\ &\equiv (E_0 + \lambda E_1 + \lambda^2 E_2 + \cdots)/N , \\ e_0(x) &= 1 + C_1 x + C_2 x^2 \ln(x^2) + \cdots , \\ e_j(x) &= 1 + K_{1j} x + K_{2j} x^2 \ln(x^2) + \cdots \quad (j = 1,2,\ldots) , \\ \alpha_j &\equiv a_j / a_0 , \end{aligned} \tag{6}$$

with $x \equiv (\rho a_0^3)^{1/2}$. The K_{ij} $(i=1,2;\ j=1,2,\ldots)$ can be expressed in terms of the α_j's and C_i's of (2) by algebraic manipulation. This was done with the computer algebra package software system MACSYMA.[10] Note that while (2) is based on the ideal Bose gas as the reference system, the reference system in (6) is the nontrivial fluid of repulsive spheres with scattering length a_0. Whereas the energy per particle as given by (2) was 9 orders of magnitude too large compared with both laboratory and computer experimental results (Fig. 1), the partial sums of (6) (giving the energy to orders zeroth through sixth) are found to be already within only one order of magnitude of the experimental results, but still too disparate and chaotic in behavior at physical densities to be considered a meaningful result. We shall refer to the rearranged energy-per-particle series (6) as a quantum thermodynamic perturbation theory (QTPT). The various ways of splitting the selected pair potentials according to (4) are now described.

III. PAIR POTENTIALS AND PARTITIONINGS

Several potentials have been proposed to model the interaction of two He atoms. One is the two-parameter Lennard-Jones (LJ) 6-12 with the parameters of de Boer and Michels.[11] Phase-shift equivalent to this potential is the three-parameter hard-core square-well (HCSW) designated designed by Burkhardt.[12] Finally, the Aziz potential designated HFDHE2 (Ref. 13) contains a few more parameters but is considered perhaps the most realistic He-He potential yet devised.

While the HCSW is a rather simplistic model of a two-particle interaction, it has the redeeming feature of admitting a closed, analytical expression for the S-wave scattering length. To find this expression, one simply solves the zero-energy, $l=0$ radial two-body Schrödinger equation,

$$u_0''(r) = v(r) u_0(r) , \tag{7}$$

where $v(r) \equiv (m/\hbar^2) V(r)$. Applying the usual boundary conditions for the distinct regions of the HCSW to the wave function leads to

$$\begin{aligned} a/c &= \left[1 + \alpha \left[1 - \frac{\tan\sqrt{\lambda}}{\sqrt{\lambda}} \right] \right] \\ &= 1 - \alpha(1/3\lambda + 2/15\lambda^2 + \cdots) , \end{aligned} \tag{8}$$

where $\alpha \equiv (R-c)/c$, R is the width of the attractive square well, $-V_0$ its depth, c the repulsive core diameter, and $\lambda \equiv (m/\hbar^2) V_0 (R-c)^2$. Unfortunately, with the more realistic LJ and Aziz potentials there is no longer

an analytic expression for a, nor an exact expansion in powers of λ, but numerical methods[14] can be used to determine both a and its expansion coefficients. In addition to being potential-shape dependent, the coefficients in (10) will also depend on how one chooses to split the potential into "reference" plus "attractive" parts, as we shall now see.

The zero-energy S-wave reduced radial wave function $u_0(r)$ must still satisfy (7), with the boundary conditions

$$u_0(0)=0 \quad \text{and} \quad \lim_{r\to\infty} u_0(r)=r-a \ . \tag{9}$$

Then (7) and (9) can be cast[14] into the integral form

$$u_0(r)=r-\int_0^r dr' r' v(r') u_0(r') - r\int_r^\infty dr' v(r') u_0(r') \ . \tag{10}$$

In the limit of $r\to\infty$, this together with (9) gives the convenient integral representation

$$a=\int_0^\infty dr\, r v(r) u_0(r) \ . \tag{11}$$

Therefore, having an expansion for $v(r)$ and $u_0(r)$ in powers of λ leads directly to an expansion for a in terms of λ. Thus, writing

$$u_0(r)=\sum_{k=0}^{\infty}\frac{\lambda^k}{k!}u_{0k}(r) \tag{12}$$

and combining this with (4) and (7) yields

$$v(r)u_0(r)=\sum_{n=0}^{\infty}\frac{\lambda^n}{n!}[v_{\rm ref}(r)u_{0n}(r)+nv_{\rm att}(r)u_{0n-1}(r)] \ . \tag{13}$$

Taylor expanding a about $\lambda=0$ gives

$$a=\sum_{n=0}^{\infty}\frac{\lambda^n}{n!}\left[\frac{d^n a}{d\lambda^n}\right]_{\lambda=0} , \tag{14}$$

and comparing (11), (13), and (14) then yields

$$\left[\frac{d^n a}{d\lambda^n}\right]_{\lambda=0} = \int_0^R dr\, r v_{\rm ref}(r)u_{0n}(r) + n\int_R^\infty dr\, r v_{\rm att}(r)u_{0n-1}(r) \ . \tag{15}$$

Thus, all that remains is to find the $u_{0n}(r)$, $n=0,1,2,\ldots$. This may be accomplished either by using the differential (7) or the integral (10) equations for $u_0(r)$. For r values inside the repulsive core the following approach is useful. From (7) and (13) we have

$$u''_{0n}(r)=\begin{cases} v_{\rm ref}(r)u_{0n}(r), & r\le R \\ nv_{\rm att}(r)u_{0n-1}(r), & r\ge R \end{cases} , \tag{16}$$

where R is the distance one chooses at which to split the potential. Again, demanding continuity of the wave function at $r=R$, one finds that *inside* the repulsive core the $u_{0n}(r)$ are proportional to each other if $u_{0n}(0)=0$, which in turn is required for all n since the *total* radial wave function (12) must vanish at $r=0$. Numerical integration was used to obtain $u_{00}(r)$ with the additional condition $[u'_{00}(r)]_{r=R}=1$. Then, in accordance with the second equation of (9) we have

$$u_{00}(r)=r-a_0 \quad (r\ge R) \ . \tag{17}$$

To find $u_{0n}(r)$ *outside* the repulsive core, begin with (10) and (12) and collect like powers of λ to obtain

$$u_{0n}(r)=-n(r-a_0)\int_r^\infty dr' v_{\rm att}(r')u_{0n-1}(r') - n\int_R^r dr'(r'-a_0)v_{\rm att}(r')u_{0n-1}(r') \ . \tag{18}$$

Finally, with $u_{00}(r)=r-a_0$ for $r>R$, one can generate all the $u_{0n}(r)$ and therefore, using (15), as many coefficients to the expansion (14) as desired. The importance played by the choice of R in these calculations is clearly evident.

A variety of ways of dividing a potential function $V(r)$ have been proposed in the literature and are illustrated in Fig. 2 for the LJ potential. In the right half of the figure, the thick curves represent the reference potential $V_{\rm ref}(r)$ of Eq. (4), and the thin curves the remaining attraction $V_{\rm att}(r)$. One of the earliest partitionings, proposed by McQuarrie and Katz[15] (MK), simply divides the potential into its negative (r^{-6}) and positive (r^{-12}) parts. Barker and Henderson[16] (BH) suggested a splitting at the zero of the *potential* energy function, say $r=\sigma$, while Andersen, Chandler, and Weeks[17] did so at the zero of the *force* ($-\partial V/\partial r$), say $r=r_0$. The WCA method splits the potential at its minimum and the portion of $V(r)$ for $r<r_0$ is shifted up by a constant positive amount ϵ so that the $r>r_0$ portion of $V(r)$ may be continued smoothly down to $r=0$ along the constant value $-\epsilon$. An even earlier method (known as the "separation method" in nuclear physics) was proposed by Moszkowski and Scott[18] (MS). It splits the potential at a distance d where the leading coefficient in the expansion (5) vanishes, thus cancelling the effect of the strong repulsion with part of the attraction. Still another scheme recently proposed by Kang, Ree, and Ree[19] suggests treating the splitting distance R as a variable parameter. This is displayed in Fig. 3 for the Aziz potential, and will be designated as Aziz INT. Note that $V_{\rm ref}(r)$ has been shifted upward by the constant amount $|V(R)|$, as in the WCA scheme.

The MS splitting was originally judged promising

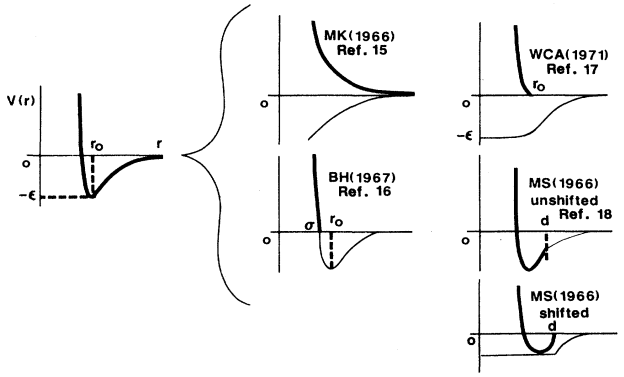

FIG. 2. Different methods of partitioning a typical pair potential like the Lennard-Jones potential, as discussed in the text.

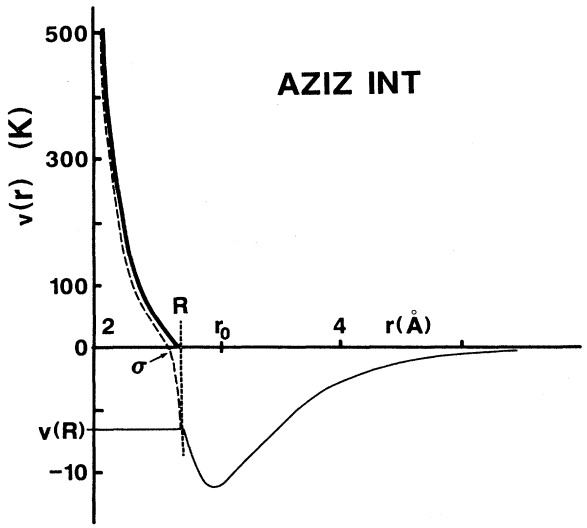

FIG. 3. The partitioning scheme intermediate (INT) between the BH and WCA schemes, for the Aziz potential (dashed curve). Thick curve refers to $V_{\rm ref}(r)$, and thin to $V_{\rm att}(r)$, defined in Eq. (4). The value for R is between σ and r_0, the zeros of the potential and force of the Aziz interaction, respectively.

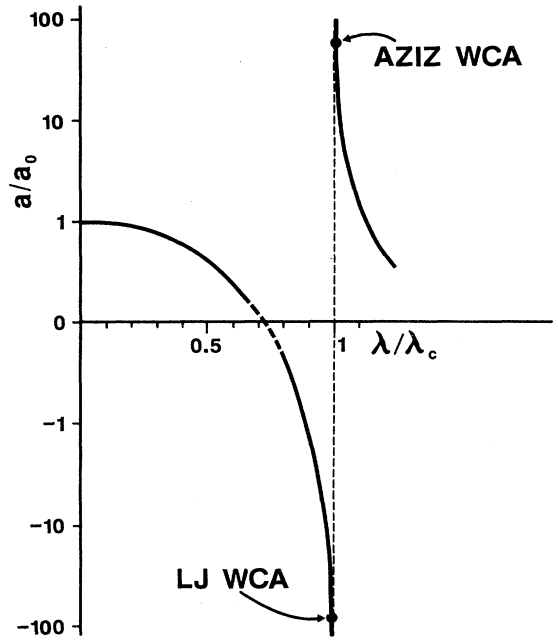

FIG. 4. Schematic behavior of the scattering length a (in units of a_0) as a function of λ/λ_c, where λ_c is the critical value of λ in Eq. (4) needed to produce a zero-energy bound state. The dots give the actual values for both the LJ and Aziz potentials, partitioned via the WCA scheme.

since, unlike all the other methods, it incorporates some of the attraction into the reference potential. However, it proved to be a discouraging surprise. If the leading term a_0 in the series (5) for a is zero, the rearranged expansion (6) is trivially zero since then $x \equiv (\rho a_0^3)^{1/2} = 0$. Shifting the potential (à la WCA), gives a nonzero positive a_0. With this "shifted-MS" scheme, however, our equation-of-state QTPT calculations eventually gave overbinding in liquid ^{4}He by a factor of *3* or so, at more than *twice* the equilibrium density, as compared with empirical equilibrium values. The reason for this is perhaps traceable to the *shape* of the reference potential (see Fig. 2, thick solid curve, lower right-hand corner): the artificial attractive "pocket" surrounding the main repulsion probably induces binding of tight clusters of particles, thus yielding unrealistically large both overall binding per particle and equilibrium density.

On the other hand, the BH potential splitting may be excluding from the reference potential a significant repulsive component of the *force* (an important factor in determining the liquid structure). The particles thus appear smaller than they actually are and this overestimates the equilibrium density. The WCA formulation corrects for this by including *all* of the repulsive force within the reference potential. Determination of the classical radial pair distribution function $g(r)$ near triple-point densities and temperatures has shown[20] that for the LJ interaction the WCA splitting best reproduces the $g(r)$ calculated via molecular-dynamics computer simulations. We are unaware of any corresponding definitive results for the Aziz interaction. These observations, valid for a classical liquid, were vindicated by our quantum calculations with the LJ, but not with the Aziz, potential.

The Aziz potential is quite different from the LJ, since it supports a weakly bound ($\sim 10^{-3}$ K) state and has a "softer" repulsive core. Figure 4 is a *schematic* picture

TABLE II. Expansion coefficients (in Å units) for the scattering length a, as defined in Eq. (10), for the Aziz potential, various partitionings as defined in Eqs. (9) and (31). The starred value of $R = 2.67$ (in Å units) turned out to be the optimum one for the Aziz potential.

	BH			INT			WCA
R	2.638	2.67*	2.72	2.77	2.82	2.87	2.97
a_0	2.146 318	2.156 236	2.170 207	2.181 891	2.191 167	2.197 912	2.203 290
a_1	−2.749 828	−2.732 589	−2.707 885	−2.686 946	−2.670 215	−2.658 036	−2.648 363
a_2	−2.416 361	−2.395 563	−2.365 760	−2.340 317	−2.319 908	−2.305 036	−2.293 241
a_3	−2.422 435	−2.400 065	−2.367 886	−2.340 336	−2.318 199	−2.302 059	−2.289 265
a_4	−2.462 469	−2.439 182	−2.405 501	−2.376 645	−2.353 449	−2.336 535	−2.323 131
a_5	−2.508 168	−2.483 888	−2.448 915	−2.418 954	−2.394 874	−2.377 316	−2.363 405
a_6	−2.555 333	−2.530 173	−2.493 931	−2.462 893	−2.437 954	−2.419 775	−2.405 373

for both LJ and Aziz potentials of the scattering length[21] (in units of the leading term a_0 associated with the WCA reference potential) as functions of λ/λ_c. Here λ_c is the critical value of λ required to produce a zero-energy two-body bound state, and is $\simeq 1.01$ for LJ and $\simeq 0.98$ for Aziz, see Table I. For the HCSW case (8), λ_c is clearly just $\pi^2/4$, the first pole of $\tan\sqrt{\lambda}$ for positive $\sqrt{\lambda}$. For the Aziz potential neither BH nor WCA splittings turned out to be adequate and we were forced to employ the "intermediate" (INT) partitioning of Kang, Ree, and Ree.[19] Table II lists the first six terms in the second member of (5), in Å units, found numerically for the Aziz potential using the results of this section with the BH, WCA, and int potential splittings using the R values, in Å units, indicated. Note that since the Aziz potential has a bound state, the series (5) *diverges;* however, [5/5](λ) Padé summation [see below, Eq. (19)] employing the first ten coefficients a_i of *any* of the seven columns of Table II gives the total a value quoted in Table I to at least seven digits.

The problem of the slow convergence (or even divergence) at physical densities of the low-density series (6) remains, and in the next section we examine how Padé extrapolants (both standard and generalized) can be advantageously applied to remedy this.

IV. DENSITY SERIES EXTRAPOLATION

A method is needed for extrapolating to physically relevant densities the various low-density series $e_i(x)$ of (6). One such technique is the well-known method of Padé approximants.[22] The Padé approximant $[L/M](x)$ to a given Taylor series $f(x)=f_0+f_1x+f_2x^2+\cdots$ is defined as the ratio of two polynomials in x, the numerator being of order L and the denominator of order M, namely

$$[L/M](x)\equiv\frac{1+p_1x+p_2x^2+\cdots+p_Lx^L}{q_0+q_1x+q_2x^2+\cdots+q_Mx^M}\equiv\frac{P_L(x)}{Q_m(x)}\ , \tag{19}$$

such that $[L/M](x)-f(x)\equiv O(x^{L+M+1})$. Clearly, binomial expansion of the denominator of (19) about $x=0$ leaves a power series identical through order x^{L+M} to the original power series. The advantage of a rational approximant is its ability to mimic nontrivial *zeros* and *poles* of the unknown function $f(x)$. Padé approximants have been shown to accurately reproduce a given function even out to values of x where the original Taylor series to the function no longer converges. They have even been found useful in representing functions with *diverging* Taylor series. Here, Padé approximants are applied to the power series in the coupling parameter λ, and generalized for the nonpower series in the density variable x.

Generalized Padé approximants can be constructed for the nonpower density series,

$$e_j(x)=1+K_{1j}x+K_{2j}x^2\ln(x^2)+K_{3j}x^2+\cdots \quad (j=0,1,2,\ldots)\ , \tag{20}$$

where $x\equiv(\rho a_0^3)^{1/2}$, and where the K_{3j} coefficients are unknown. In this case, instead of having a pure polynomial in both the numerator and the denominator of the approximant as in (19), *one* of these will contain a $\ln(x^2)$ term. Since only the K_{1j} and K_{2j} coefficients are known, the series in (20) is initially truncated with only the three terms,

$$e_j(x)=1+K_{1j}x+K_{2j}x^2\ln(x^2)+\cdots\ . \tag{21}$$

All possible generalized Padé approximants to this series must be constructed, which is accomplished by applying an extrapolation scheme called "tailing."[23] This yields four unique generalized Padé approximants plus the original series. The approximants to $e_j(x)$ (21) will be denoted by $\epsilon_j(x)$. They are listed in Table III and designated as 0, *i*, *ii*, *iii*, *iv*. These constitute the so-called "small" family of extrapolants.

In a few select cases, these density extrapolants fail to provide a suitable representation which is compatible with known overall properties of the exact (but unknown) $\epsilon_j(x)$, viz., positivity, monotonicity, singularity structure, etc. However, certain global constraints, to be described shortly, allow fixing the next coefficient (K_{3j}) of the series (20), thus providing us with a large family of approximants. Applying the same "tailing" techniques to the resulting four-term series (20) yields 12 forms of which only 11 are distinct. These are listed in Table IV. They will be referred to as the "large" family of extrapolants, and designated as I, II, . . . , XII, with I≡V. Ideally, whether dealing with the "small" $(0,i,\ldots,iv)$ or "large" (I,II, . . . , XII) family of extrapolants, all but *one* of these forms should be eliminated before the final energy calculations can be performed. Other methods exist for constructing Padé-like approximants to a nonpower series,[24] and may be useful in eliminating extra extrapolants in cases where more than one survive the initial screening.

The very first step in the density extrapolation problem is to find a suitable extrapolant for the reference fluid.[25,26] Since $e_0(x)$ in (6) represents the unperturbed energy it may be thought of as the energy of a system of pure hard spheres of diameter a_0 with no attraction. Several impor-

TABLE III. "Small" family of extrapolants, to a *three*-term series of the form (21). Each approximant is of the form $M+N(x)/D(x)$, which by definition reduces to (21) on expansion about $x=0$. The terms $N(x)$ and $D(x)$ will depend on whether $M=0$ or $M=1$ (Compare, e.g., forms *i* and *iv*).

Form	M	$N(x)$	$D(x)$
0	0	$1+K_1x+K_2x^2\ln x^2$	1
i	1	K_1x	$1-K_2x^2\ln x^2/K_1$
ii	0	1	$1-K_1x-K_2x^2\ln x^2$
iii	0	$1+K_2x^2\ln x^2$	$1-K_1x$
iv	0	$1+K_1x$	$1-K_2x^2\ln x^2$

TABLE IV. "Large" family of approximants, to the *four*-term series of the form (20), of the same form $M+N(x)/D(x)$ as in Table III. Note that form V is identical to form I.

Order	M	$N(x)$	$D(x)$
I	1	$K_1x+K_2x^2\ln x^2$	$1-K_3x/K_1$
II	1	$K_1x+K_3x^2$	$1-K_2x\ln x^2/K_1$
III	1	K_1x	$1-K_2x\ln x^2/K_1-K_3x/K_1$
IV	0	$1+(K_1-K_3/K_1)x$	$1-K_3x/K_1-K_2x^2\ln x^2$
V=I	0	$1+(K_1-K_3/K_1)x+K_2x^2\ln^2$	$1-K_3x/K_1$
VI	0	1	$1-K_1x-K_2x^2\ln x^2-(K_3-K_1^2)x^2$
VII	0	$1+K_1x+K_2x^2\ln x^2$	$1-K_3x^2$
VIII	0	$1+K_2x^2\ln x^2+(K_3-K_1^2)x^2$	$1-K_1x$
IX	0	$1+K_1x+K_3^2x$	$1-K_2x^2\ln x^2$
X	0	$1+K_1x$	$1-K_2x^2\ln x^2-K_3x^2$
XI	0	$1+K_2x^2\ln x^2$	$1-K_1x-(K_3-K_1^2)x^2$
XII	0	$1+(K_3-K_1^2)x^2$	$1-K_1x-K_2x^2\ln x^2$

tant qualitative characteristics of the behavior that the appropriate extrapolant $\epsilon_0(x)$ must possess may be delineated. First, the maximum packing density for identical spheres of diameter c is well known to be $\rho_0\equiv\sqrt{2}/c^3$, corresponding to so-called primitive-hexagonal packing (of which face-centered-cubic and hexagonal-close packing are two examples). The maximum *physical* value of $x=(\rho c^3)^{1/2}$ is thus $x_0=(\rho c^3)^{1/2}=(\sqrt{2})^{1/2}\simeq 1.1892$. Consequently, one expects a pole in $\epsilon_0(x)$ near, if not precisely at, this value of x. The uncertainty principle requires that as density is increased and perfect spatial localization of each sphere is approached, the energy should diverge as the $\frac{2}{3}$ power of the available volume. Therefore the pole in x must be of second order. To obtain this second-order pole one may analyze the density series for $e_0(x)$ in (6) raised to the power $-\frac{1}{2}$, construct its Padé approximant, and search for a possible zero of this extrapolant. Thus, instead of $e_0(x)$ as given in (6), we start from

$$e_0^{-1/2}(x)=1-\tfrac{1}{2}C_1x-\tfrac{1}{2}C_2x^2\ln(x^2)+\cdots . \tag{22}$$

A second requirement is that the extrapolant to $e_0^{-1/2}(x)$, say $\epsilon_0^{-1/2}(x)$, must not increase faster than linearly in x, so as to guarantee that the hard-sphere energy $E/N\equiv(2\pi\hbar^2/mc^2)x^2\epsilon_0(x)$ increase monotonically in x, as it should. Graphing the five possible extrapolants to (22), called 0, *i*, *ii*, *iii*, and *iv* and listed in Table III, one sees that only *one* of the five extrapolants (form *i*) satisfies the condition of not increasing faster than linearly in x as well as having a zero near $x_0=(\sqrt{2})^{1/2}\simeq 1.1892$. (See Fig. 1, Ref. 26). Additionally, as Fig. 5 shows, this form (*i*) lies reasonably close to the GFMC (Ref. 27) data points (dots) for boson hard spheres and has the same curvature.

In an attempt to reproduce the boson hard-sphere GFMC data more closely, the Padé extrapolants to the *four*-term series are analyzed, where the next successive term in (22), $-\frac{1}{2}(C_3-C_1^2/4)x^2$, with C_3 unknown, is included. The resulting 11 distinct forms (Table IV) were then examined[26] but only *two* were found to be acceptable, based on the criterion that the GFMC data points be mapped onto as straight a line as possible, with the *slope* of the line determining the value of the unknown C_3 coefficient. These two forms are marked "II" and "III" in Fig. 5. Also displayed (crosses) are results of previously mentioned parquet-diagram calculations[3] for the boson hard-sphere system. Form III turned out to have a much smaller root-mean-square deviation from the GFMC data points, and explicitly leads to

$$\epsilon_0(x)=\left[\frac{1}{1+\dfrac{K_1x}{1-(K_2/K_1)x\ln(x^2)-(K_3/K_1)x}}\right]^2 \tag{23}$$

with $K_1=-\frac{1}{2}C_1$, $K_2=-\frac{1}{2}C_2$, and $K_3=-\frac{1}{2}(C_3-C_1^2/4)$. The value $C_3=25.11\pm0.287$ was determined[26] by a smallest least-mean-squares fit of the aforementioned straight line to the GFMC data, and the resulting pole placement predicted is $x_p=0.7245\pm0.0045$. From Fig. 5 it is hard to imagine how the GFMC data could extrapolate to a pole anywhere near the primitive-hexagonal packing value $x_0\simeq 1.1892$. It is tempting to speculate

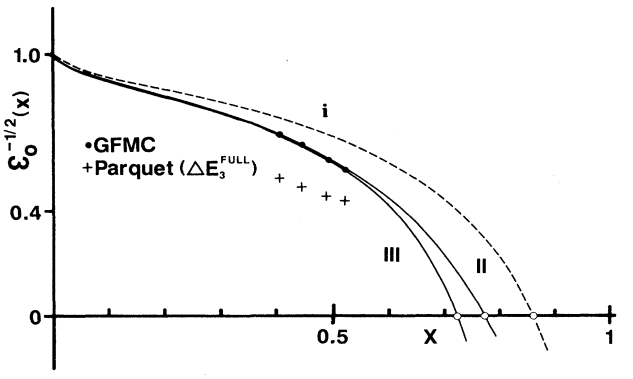

FIG. 5. Possible choices for the zero-order hard-spheres extrapolant to Eq. (22). Here *i* refers to the best unconstrained extrapolant from the "small" family, while II and III are the members of the "large" family with C_3 chosen to reproduce the slope of GFMC data for pure hard spheres, as detailed in Ref. 27. Crosses refer to calculations of Ref. 3.

TABLE V. Value of $\epsilon_j(x_p)$ for LJ WCA. [P is the pole in the physical interval; *, the best Stell-Penrose (SP) behavior]. The values in column 1 should be compared with the estimate from Eq. (25) of 2.9954 for the Burkhardt HCSW potential which is phase-shift equivalent to the LJ potential.

Form	Order j	1	2	3	4	5	6
0		−16.88	33.95	19.95	−5.88	−36.1	−62.3
i		3.153*	0.96*	−0.26*	−6.49	*P*	*P*
ii		0.083	*P*	*P*	0.13*	0.026*	0.01*
iii		*P*	15.84	3.59	0.35	−2.09	−4.6
iv		0.352	*P*	*P*	*P*	−0.37	−0.16

that the pole reproduced by (23) might correspond to a lower-density, "random" close-packing configuration. The energy per particle (in degrees kelvin) associated with the form (23) is shown as the thick solid curve marked HS (for hard spheres) in Fig. 1. Also displayed there are the hard-sphere GFMC data points of Ref. 27 (solid squares).

Four additional global criteria (or "boundary conditions") may be invoked to allow for a systematic elimination of all but one form in each successive perturbative order beyond the zeroth. (1) We demand that the density extrapolant $\epsilon_i(x)$ ($i=1,2,\ldots$) be free from poles in the "physical interval" $0\le x\le x_p$. (2) Since E_1 and E_2 in (6) must be negative[25] for all densities, and since a_1, a_2 in (6) are always negative, acceptable approximants $\epsilon_1(x)$ and $\epsilon_2(x)$ to the series $e_1(x)$ and $e_2(x)$, respectively, must be *positive* for all x in the physical interval. (3) Furthermore, since the first-order energy contribution E_1, being an expectation value, is just an integral over a probability density that can only *increase* as the particles crowd together more and more, the first-order extrapolant $\epsilon_1(x)$ must be monotonically increasing in the density. (4) *Classical* thermodynamic perturbation theory to first order has rigorously been proved[28] to be *exact* at close packing in one and two dimensions. Moreover, Stell and Penrose conjectured[28] it to hold in three dimensions as well. Assuming it holds also in the *quantum* case, the energy at close packing is then simply given by

$$E=E_0+\lambda E_1 \ . \tag{24}$$

Therefore, in addition to having a second-order pole in x, E must depend *linearly* on the attractive well strength λ, as $x\to x_p$. In view of (6) this means that $E_2=E_3=\cdots=0$, as $x\to x_p$, implying that $\epsilon_2(x_p)=\epsilon_3(x_p)=\cdots=0$. We shall refer to these relations as the Stell-Penrose (SP) conditions.

Indeed, we found that the extrapolants eventually chosen for third and higher order at close packing had very nearly the ideal value of zero. Second order was less well behaved, so the condition $\epsilon_2(x_p)=0$ was imposed by determining the unknown constant K_{32} of (20) in each approximant (Table IV), and selecting the one which best satisfied the other criteria.

For most orders, however, the smaller family ($0-iv$) (Table III) already provided *one* suitable extrapolant, with the rest eliminated. Table V gives an example where all orders required only "small family" approximants, where the asterisks identify the form chosen in each perturbative order. In second order, even though the "best" extrapolant (*i*) did not satisfy the SP conditions $\epsilon_2(x_p)=0$, the large family of extrapolants yielded a form (III) that closely resembled the form *i*. We tested this choice by employing a method similar to that used for the zero-order extrapolant. Namely, an exponent is introduced which is varied to ensure compliance with the SP conditions. This yielded a third extrapolant which was nearly identical to the forms *i* and III over most of the range of x values in the physical interval. A notable exception to these general trends occurred in fourth order for the Aziz potential with any partitioning scheme. This order necessitated incorporating the fourth coefficient K_{34} into the density series (21).

As regards first order, a rough estimate[29] of the attractive potential energy contribution for the hard-core square-well potential shape of depth $-V_0$, range R, and hard-core diameter c, is just

$$\lambda E_1/N=-\tfrac{1}{2}V_0(\tfrac{4}{3}\pi R^3\rho_p-1) \ , \tag{25}$$

where the term in parentheses is the number of hard-sphere centers between two concentric spheres of radii R and c (i.e., inside the attractive well of the HCSW potential). By equating the above to the $j=1$ term in (6) one can obtain an estimate for the value of the first-order extrapolant at close packing, depending on the parameters of the HCSW. As a reassuring check on the approximants chosen, the first order extrapolant at $x=x_p$ for either the LJ or the Aziz potentials with any given splitting produced a result at $x=x_p$ very nearly equal to that predicted by the estimate[29] for the Burkhardt He-He HCSW potential. Approximant forms thus chosen for LJ-BH, Aziz-INT, and Aziz-INT are displayed in Figs. 6, 7, and 8, respectively, and will be discussed later.

V. RESULTS AND DISCUSSION

Once good density extrapolants $\epsilon_j(x)$ are constructed to each $e_j(x)$ in the QTPT energy expression (6), the resulting series for the ground-state energy per particle

$$E/N=\frac{2\pi\hbar^2}{ma_0^2}x^2\epsilon_0(x)\left[1+\sum_{j=1}^{\infty}\alpha_j\frac{\epsilon_j(x)}{\epsilon_0(x)}\lambda^j\right] \tag{26}$$

may be analyzed as a λ series. Note that $e_0(x)$ and $e_j(x)$ have been replaced by their extrapolant forms $\epsilon_0(x)$ and $\epsilon_j(x)$. One can then investigate the density behavior of the series in brackets to a given finite order in λ, say

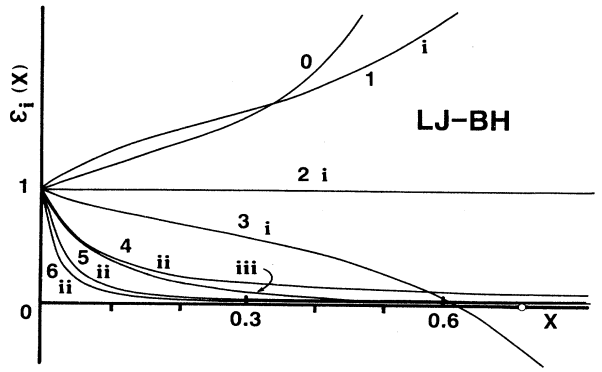

FIG. 6. Chosen extrapolants to the $e_j(x)$ of Eq. (6) for the LJ potential, BH partitioning. Of the two forms shown for fourth order, *iii* is retained as it conforms better to the Stell-Penrose (SP) conditions discussed in the text.

$L+M$, by studying the behavior of the different $[L/M](\lambda)$ approximants for $\lambda=\lambda_{\text{physical}}$. The latter value is $(m/\hbar^2)V_0(R-c)^2$ for the HCSW, and unity for the LJ and Aziz interactions.

Energy calculations were initially performed for the HCSW with the potential parameters deduced by Burkhardt[12] so that we could utilize the analytic expression (8) for the scattering length. Burkhardt determined the potential parameters by demanding that the HCSW give phase shifts equivalent (at least in the first few partial waves) to those of the LJ potential. Unfortunately, as is well known, *two*-body phase-shift-equivalent potentials may give rise to substantially different *many*-body properties. In addition to this, the LJ interaction is now considered only a moderately accurate description of the two-body interaction for He atoms. Energy results obtained for the Burkhardt HCSW potential have been reported elsewhere.[29] Not surprisingly, they were poor when compared with experiment or GFMC, but it was clear that the QTPT method was converging very rapidly as of fifth order in λ. This suggested taking the potential parameters of the HCSW and modifying them systematically subject only to an observed requirement[30] on the

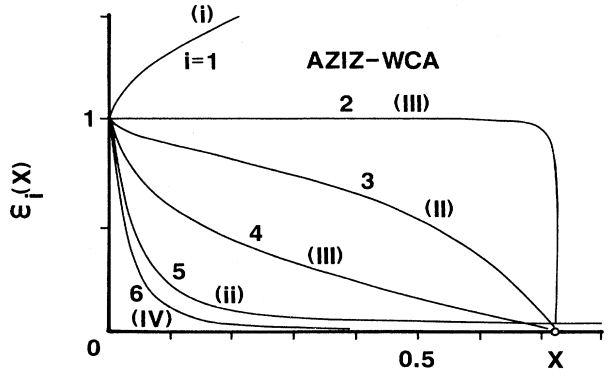

FIG. 7. Same as Fig. 6 but for the Aziz potential, WCA partitioning.

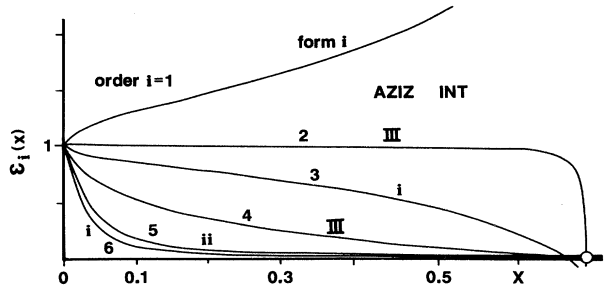

FIG. 8. Same as Fig. 6 but for the Aziz potential, INT partitioning scheme.

magnitude of the S-wave scattering length, namely that $|a|>20$ Å for ^{4}He. This bound is in effect an empirical constraint on the parameters c, R, V_0 of the HCSW potential. These parameters were varied, making the potential shallower (smaller V_0) and the attraction longer ranged [larger $(R-c)$], but keeping $\alpha\equiv(R-c)/c$ constant. We found that the discrepancy with experiment (i.e., the error) in either the equilibrium energy per particle *or* density could separately be reduced essentially to zero. Alternately, the error in both quantities could be minimized to approximately 3%. Specifically, at an equilibrium density of 0.0218 Å^{-3}, an energy of -7.78 K was obtained. Or, an energy of -7.14 K results at an equilibrium density of 0.0230 Å^{-3}. Finally, an energy of -7.35 K was achieved at 0.0225 Å^{-3}. These should be compared to the experimental values[31] of -7.14 K at 0.0218 Å^{-3} for liquid ^{4}He. The only point of this exercise was to determine if a reasonable model pair potential, with parameters not incompatible with the two-body empirical constraint $|a|>20$ Å, could lead to QTPT results which (a) converged reasonably fast, and (b) were not too different from experiment. The result was affirmative.

To improve upon the model HCSW potential, the LJ interaction was used next. Energy-per-particle calculations were performed using both BH and WCA splittings of the potential. For this pair interaction the *small* family of extrapolants gave a suitable form in each order. In other words, at least one form was pole free in the physical interval $0<x<x_p=0.7245$ spanned by (23). These are displayed for the LJ-BH case for orders 0–6 in Fig. 6 where the labels *i*, *ii*, and *iii* refer to the specific members of the small family of approximants, Table III, to the series $e_j(x)$ in (6). The curve labeled "0" is just (22). The BH partitioning gave good agreement[32] with the GFMC (Ref. 33) data points in both energy and density, with an energy of -6.808 K at $\rho=0.0235$ Å^{-3}, for the $[6/0](\lambda)$ Padé approximant corresponding to straight sixth-order QTPT, to be compared to the GFMC values of -6.848 ± 0.018 K at a density of 0.022 Å^{-3}. As expected,[20] the WCA partitioning yielded even better agreement with the GFMC data points. The WCA splitting also gave a smaller density, as compared with BH splitting. As discussed previously, BH omits a significant portion of the repulsive force, therefore making the particles appear smaller and resulting in a larger equilibrium density than with the WCA splitting. The WCA scheme for the

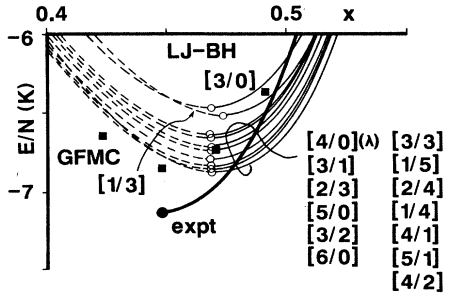

FIG. 9. Ground-state energy per particle as a function of $x \equiv (\rho a_0^3)^{1/2}$ for the LJ potential, BH partitioning. Curves labeled $[L/M](\lambda)$ refer to the L/M Padé approximants to the $L+M$ partial sum of the λ series, Eq. (26). The open circles mark the minimum of the curve. The dashed part of the curve is the metastable portion of the equation of state resulting from a Maxwell-like construction. Squares refer to the GFMC data. Solid thick curve is experimental, with the dot referring to the equilibrium density.

LJ liquid gave[32] -6.85 K at an equilibrium density of 0.0227 Å^{-3}. Results for the LJ potential (BH and WCA) are summarized in Table I of Ref. 32. Figure 9 displays the behavior of several λ-Padé approximants $[L/M](\lambda=1)$ to several $L+M \leq 6$ partial sums of (26) for the LJ-BH case, with the open circles marking the location of the predicted equilibrium minima. Squares designate GFMC data points and the thick curve represents the experimental equation of state.[31]

Computer simulations[34] with the Aziz interaction have reproduced experimental liquid ^{4}He results very closely. Several differences are apparent between the LJ and Aziz potentials which will be significant in our calculations. First, there is the relative hardness of their repulsive cores.[35] At $r=0$ the value of the LJ potential is infinite, while the Aziz potential has a value which although very

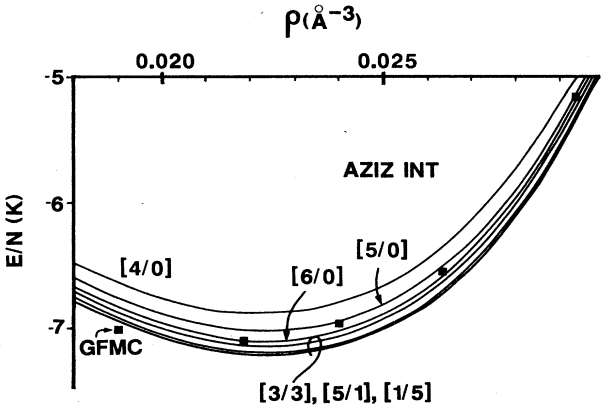

FIG. 10. Equation of state for the Aziz potential, int partitioning with $R=2.67$ Å, as a function of particle density ρ in units Å^{-3}. Curves labeled $[L/M](\lambda)$ refer to the L/M Padé approximants to the $L+M$ partial sum of series, Eq. (26). Squares refer to the GFMC data points.

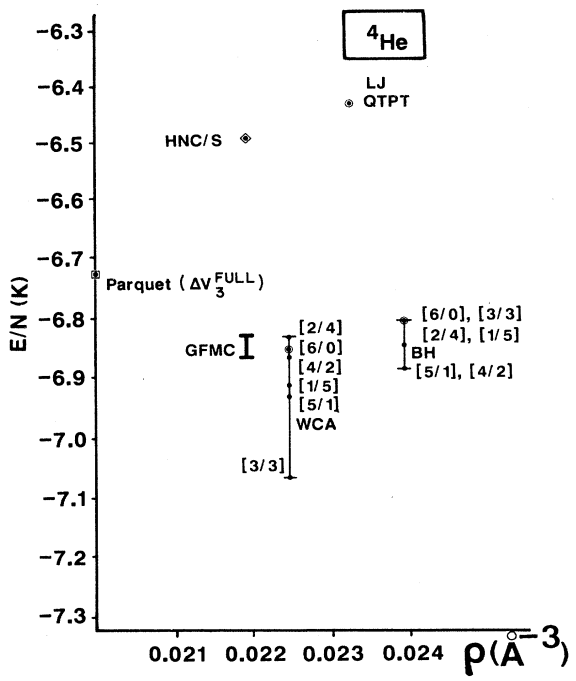

FIG. 11. Summary of equilibrium energy-density results for the LJ potential. HNC/S refers to the calculations of Ref. 36, parquet to those of Ref. 3, GFMC data are from Ref. 33. The $[6/0](\lambda)$ Padé (circled dots) correspond to straight sixth-order QTPT; other dots refer to other sixth-order Padé results to the λ series (26).

large ($\sim 5.88\times10^6$ K) is nevertheless finite. Also, the Aziz potential exhibits a very weakly bound state ($\sim 10^{-3}$ K) which the LJ does not (see Fig. 4).

To examine the implications of the relative core hardness, recall the form (23) of the extrapolant $\epsilon_0(x)$ used. This form was determined with *hard-sphere* GFMC data as a guide. While this may be adequate for the LJ liquid, the softness of the Aziz potential core must be compensated for in applying this approach. From the earlier discussion in Sec. III, the BH partitioning was faulted for excluding too much of the repulsive force from the reference potential. In the case of the Aziz potential, this is exactly what is needed in its hard-sphere reference system. (Of course, BH may still exclude too much of the repulsion.) Therefore, the method of Kang *et al.*[19] was also applied where the partitioning distance R is variable. The extremes of the interval of interest are chosen to be $R=\sigma$, the zero of the potential (which is just the BH partitioning) and $R=r_0$, the minimum of the potential (just the WCA partitioning). The Kang *et al.* partitioning is intermediate (INT) between these two extremes. Specifically, we have

$$R = \begin{cases} \sigma & \text{(BH)} \\ r_0 & \text{(WCA)} \end{cases} \qquad (27)$$

$$\sigma < R < r_0 \quad \text{(INT)} .$$

For the Aziz potential $\sigma=2.638$ Å and $r_0=2.97$ Å. The

interval (σ, r_0) is divided into five parts, beginning at 2.67 Å and increasing by 0.05 Å to include the values $R = 2.72$, 2.77, 2.82, and 2.87 Å. The scattering length coefficients were determined using the methods of Sec. III for each of these R values and are reported in Table II.

In addition, while the LJ-BH $\epsilon_i(x)$ extrapolants Fig. 6 exhibited approximate SP behavior [i.e., $\epsilon_i(x_p) \simeq 0$ for $i = 3, \ldots$] in all (third and higher) orders with the *small* family of forms, the Aziz extrapolants in fourth order for *all* potential partitionings were poorly behaved. Thus for the Aziz pair potential the *large* family of extrapolants was needed. Only one of the remaining fourth-order extrapolants was smoothly decreasing, and thus retained. For the Aziz WCA case we also used the large family of extrapolants to analyze second, third, and sixth order as well. (Interestingly enough, only one of the second-order forms exhibited behavior very similar to that of the small family optimum extrapolant, staying relatively constant over the density region of interest.) This is displayed in Fig. 7 for orders 1–6.

Similarly, the chosen extrapolants for the best intermediate splitting of the potential (referred to as Aziz INT) are shown in Fig. 8 for the splitting value $R = 2.67$ Å; this is very close to the BH value of $R = \sigma = 2.638$ Å for the Aziz potential. Figure 10 shows the resulting equation of state (26) for Aziz INT as given by fourth-, fifth-, and sixth-order straight QTPT ([4/0], [5/0], [6/0], respectively). All sixth-order λ-Padé approximants are shown as well, with the exception of [4/2] and [2/4] which were singular very near the equilibrium density and thus discarded. The closeness of all sixth-order ap-

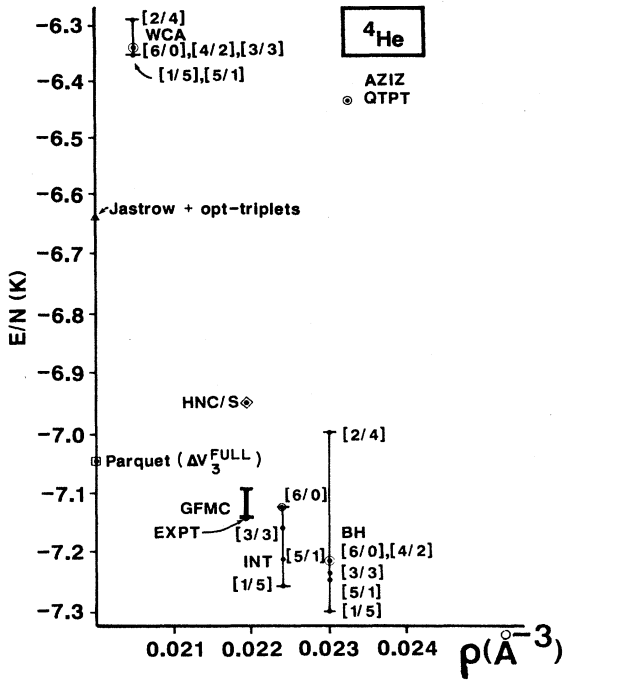

FIG. 12. Same as Fig. 11 but for the Aziz potential. The large dot marked EXPT is the laboratory experimental energy-density equilibrium point. The data marked "Jastrow+opt-triplets" refers to the calculations of Ref. 37. Neither the BH nor the WCA potential splittings gave as good an agreement with GFMC as in the LJ case and so the int splitting discussed in text was also tried.

TABLE VI. Predicted QTPT equilibrium energy per particle E/N (in degrees K) and density ρ_e [where $x_e \equiv (\rho_e a_0^3)^{1/2}$ and dimensionless] with all sixth-order Padé approximants $[L/M](\lambda)$ to the λ series (26). (a) gives the results for the LJ potential, split via BH and WCA schemes discussed in the text. (b) gives the results for the Aziz potential, split into reference plus attraction according to the three schemes discussed in text, namely BH, WCA, and INT. The bottom rows give the GFMC results against which we compare our calculations. For Aziz INT, approximants [4/2] and [2/4] develop a pole in the density interval corresponding to $0.4 < x < 0.5$, and are thus discarded.

a

LJ

	BH			WCA	
L	M	x_s	E/N (K)	x_s	E/N (K)
6	0	0.468	−6.808	0.471	−6.855
5	1	0.469	−6.892	0.472	−6.932
4	2	0.469	−6.892	0.471	−6.868
3	3	0.468	−6.812	0.468	−7.070
2	4	0.469	−6.852	0.472	−6.833
1	5	0.468	−6.851	0.472	−6.916
GFMC		0.448	−6.848±0.018	0.463	−6.848±0.018

b

Aziz

		BH		WCA		INT ($R = 2.67$ Å)	
L	M	x_s	E/N (K)	x_s	E/N (K)	x_s	E/N (K)
6	0	0.475	−7.217	0.468	−6.345	0.474	−7.124
5	1	0.475	−7.248	0.468	−6.351	0.474	−7.128
4	2	0.475	−7.217	0.467	−6.344	pole $0.4 < x < 0.5$	
3	3	0.475	−7.239	0.468	−6.344	0.474	−7.162
2	4	0.475	−7.003	0.469	−6.291	pole $0.4 < x < 0.5$	
1	5	0.475	−7.302	0.468	−6.348	0.474	−7.241
GFMC		0.465	−7.12±0.024	0.484	−7.12±0.024	0.469	−7.12±0.024

TABLE VII. Sound velocities c (in m/s) calculated from sixth-order QTPT compared with GFMC results for both LJ and Aziz interactions, according to the three potential partitioning schemes BH, WCA, and int. Here, $\sigma = 2.556$ Å.

	$\rho\sigma^3$	0.365	0.401	0.438	0.490
LJ	BH	217.34	298.21	397.75	
	WCA	206.08	284.59	380.35	
	GFMC	245.8±21.0	290.54±8.74	333.1±23.7	
Aziz	BH	209.270	290.71	390.36	
	WCA	275.87	374.24	501.65	
	INT	220.95	306.74	410.22	599.03
	GFMC	227.01±40.3	307.43±52.4	394.64±83.5	568.24±152.3

proximants shows that the λ series is well converged out to this order. The results for the WCA, BH, and INT splitting are summarized in Table VI and Figs. 11 and 12. We note that the energy and density scales of both these figures coincide with the small rectangle marked in Fig. 1. Also shown in Figs. 11 and 12 for comparison are the results of other alternate calculations, namely the "parquet" method of Ref. 3, the "HNC/S" method of Ref. 36, and the "Jastrow plus optimized-triplets" method of Ref. 37.

A very stringent test of the ground-state equation of state is the predicted velocity of sound c, defined through

$$mc^2 = \frac{\partial P}{\partial \rho} , \tag{28}$$

where m is the particle mass, and the pressure P is given by

$$P \equiv \rho^2 \frac{\partial (E/N)}{\partial \rho} . \tag{29}$$

Since the expression for E/N is given as an explicit function of x, related to ρ through $x = (\rho a_0^3)^{1/2}$, (28) and (29) lead to

$$c = 22.77994 \left[\frac{1}{x} \frac{\partial}{\partial x} \left[x^3 \frac{\partial (E/N)}{\partial x} \right] \right]^{1/2} \quad (\text{m/s}) \tag{30}$$

for ^{4}He. Using MACSYMA, we evaluated this expression at several densities and the resulting values of c are compared against the GFMC results in Table VII. We see that agreement with GFMC is within the statistical errors of the latter for the Aziz INT case, for all four density points considered. This quality of agreement is not so good for Aziz BH or WCA, nor even for LJ BH and WCA, a fact perhaps in support of the int splitting of the pair potential.

VI. CONCLUSIONS

Starting with the well-known exact, low-density equation of state for a many-boson system, we are able to extrapolate this series via a quantum-thermodynamic perturbation theory to liquid densities. Through the application of Padé approximants and with a minimum of computer size and time, excellent results are obtained for both the equilibrium energy and density for the Lennard-Jones and Aziz potentials, when compared to the corresponding GFMC computer experiments.

The LJ potential with the WCA partitioning gave results almost identical to those of the computer experiments, for both the ground-state energy per particle and equilibrium density, differing by 0.1% in energy and less than 4% in density.

With the Aziz potential GFMC calculations reproduce liquid ^{4}He laboratory results very closely. Our perturbative method required for this potential a splitting scheme intermediate between the BH and WCA schemes. When adjusted to coincide in energy, the intermediate scheme predicted the equilibrium density to within 2%, and sound velocities entirely within the statistical error bars, of the GFMC data.

ACKNOWLEDGMENTS

M. de Ll. gratefully acknowledges partial support from the Junta de Andalucía (Spain). E. B. and R. G. acknowledge support from CICyT (Comisión Interministerial de Ciencia y Technología) (Spain) under Contract No. 1234/84. C. K. thanks Dr. Francis H. Ree for discussions.

*Present address: Physics Department, Kansas State University, Manhattan, KS 66506.

[1] J. W. Clark, Prog. Part. Nucl. Phys. **2**, 89 (1979), and references therein.

[2] J. G. Zabolitzky, Prog. Part. Nucl. Phys. **16**, 103 (1986), and references therein; D. M. Ceperley and M. H. Kalos, in *Monte Carlo Methods in Statistical Physics*, edited by K. Binder (Springer, Berlin, 1979).

[3] A. D. Jackson, A. Lande, R. W. Guitink, and R. A. Smith, Phys. Rev. B **31**, 402 (1985); A. D. Jackson, A. Lande, and R. A. Smith, Phys. Rep. **86**, 55 (1982).

[4] F. Coester, Nucl. Phys. **7**, 421 (1958); H. G. Kümmel, K. H. Lührmann, and J. G. Zabolitzky, Phys. Rep. **36C**, 1 (1978).

[5] R. F. Bishop and H. G. Kümmel, Physics Today **40**, March, 52 (1987).

[6] H. K. Kümmel (private communication).

[7] A. L. Fetter and J. D. Walecka, *Quantum Theory of Many Particle Systems* (McGraw-Hill, New York, 1971); H. M.

Hugenholtz and D. Pines, Phys. Rev. **116**, 489 (1959).
[8]G. A. Baker, Jr., Rev. Mod. Phys. **43**, 479 (1971). See especially Fig. 40; M. D. Miller, L. H. Nosanow, and L. J. Parish, Phys. Rev. B **15**, 214 (1977).
[9]G. Gutiérrez, M. de Llano, and W. C. Stwalley, Phys. Rev. B **29**, 5211 (1984).
[10]R. H. Rand, *Computer Algebra in Applied Mathematics: An Introduction to MACSYMA* (Pitman, London, 1984); MACSYMA © 1976, 1984, Massachusetts Institute of Technology. Enhancements © 1984, Symbolics, Inc.
[11]J. de Boer and A. Michels, Physica **6**, 945 (1938).
[12]T. W. Burkhardt, Ann. Phys. (N.Y.) **47**, 516 (1968).
[13]R. A. Aziz, V. P. S. Nain, J. S. Carley, W. L. Taylor, and G. T. McConville, J. Chem. Phys. **70**, 4330 (1979).
[14]L. P. Benofy, E. Buendía, R. Guardiola, and M. de Llano, Phys. Rev. A **33**, 3749 (1986).
[15]D. A. McQuarrie and J. L. Katz, J. Chem. Phys. **44**, 2393 (1966).
[16]J. A. Barker and D. Henderson, Rev. Mod. Phys. **48**, 597 (1976).
[17]H. C. Andersen, D. Chandler, and J. D. Weeks, Adv. Chem. Phys. **34**, 105 (1976).
[18]S. A. Moszkowski and B. L. Scott, Ann. Phys. (N.Y.) **11**, 65 (1960).
[19]H. S. Kang, T. Ree, and F. H. Ree, J. Chem. Phys. **84**, 4574 (1986); H. S. Kang, C. S. Lee, T. R. Ree, and F. H. Ree, J. Chem. Phys. **82**, 414 (1985).
[20]D. Chandler, J. D. Weeks, and H. C. Andersen, Science **220**, 787 (1983); J. D. Weeks and J. Q. Broughton, J. Chem. Phys. **78**, 4197 (1983).
[21]E. Buendía, R. Guardiola, and M. de Llano, Phys. Rev. A **30**, 941 (1984).
[22]G. A. Baker, Jr., *Fundamentals of Padé Approximants* (Academic, New York, 1974); G. A. Baker, Jr., and P. Graves-Morris, in *Encyclopedia of Math and its Applications*, edited by G.-C. Rota (Addison-Wesley, Reading, MA, 1981), Vols. 13 and 14.
[23]V. C. Aguilera-Navarro, R. Guardiola, C. Keller, M. de Llano, and M. Popovic, Phys. Rev. A **35**, 3901 (1987).
[24]A. Isihara and E. W. Montroll, Proc. Natl. Acad. Sci. (USA) **68**, 3111 (1971).
[25]G. A. Baker, Jr., M. de Llano, and J. Pineda, Phys. Rev. B **24**, 6304 (1981).
[26]V. C. Aguilera-Navarro, S. Ho, and M. de Llano, Phys. Rev. A **36**, 5742 (1987).
[27]M. H. Kalos, D. Levesque, and L. Verlet, Phys. Rev. A **9**, 2178 (1974).
[28]J. M. Kincaid, G. Stell, and E. Goldmark, J. Chem. Phys. **65**, 172 (1976); G. Stell and O. Penrose, Phys. Rev. Lett. **51**, 1397 (1983).
[29]C. Keller, V. C. Aguilera-Navarro, and M. de Llano, J. Phys. A **21**, 715 (1988).
[30]J. P. Toennies and K. Winckelmann, J. Chem. Phys. **66**, 3965 (1977).
[31]R. A. Aziz and R. K. Pathria, Phys. Rev. A **7**, 809 (1973); P. R. Roach, J. B. Ketterson, and C. W. Woo, *ibid.* **2**, 513 (1970).
[32]M. A. Solís, V. C. Aguilera-Navarro, M. de Llano, and R. Guardiola, Phys. Rev. Lett. **59**, 2322 (1987).
[33]P. A. Whitlock, D. M. Ceperley, G. V. Chester, and M. H. Kalos, Phys. Rev. B **19**, 5598 (1979).
[34]M. H. Kalos, M. A. Lee, P. A. Whitlock, and G. V. Chester, Phys. Rev. B **24**, 115 (1981).
[35]E. Buendía, R. Guardiola, and M. de Llano, At. Data Nucl. Data Tables **42**, 293 (1989).
[36]Q. N. Usmani, B. Friedman, and V. R. Pandharipande, Phys. Rev. B **26**, 6123 (1982).
[37]E. Krotschek, Phys. Rev. B **33**, 3158 (1986).